mathematics

MDPI

Article

Precision Denoising in Medical Imaging via Generative Adversarial Network-Aided Low-Noise Discriminator Technique

Turki M. Alanazi [1,*] and Paolo Mercorelli [2,*]

[1] Department of Electrical Engineering, College of Engineering, University of Hafr Al Batin, Hafr Al Batin 39524, Saudi Arabia
[2] Institute for Production Technology and Systems (IPTS), Leuphana Universität Lüneburg, 21335 Lüneburg, Germany
* Correspondence: trmalanazi@uhb.edu.sa (T.M.A.); paolo.mercorelli@leuphana.de (P.M.)

Abstract: Medical imaging is significant for accurate diagnosis, and here, noise often degrades image quality, thus making it challenging to identify important information. Denoising is a component of traditional image pre-processing that helps prevent incorrect disease diagnosis. Mitigating the noise becomes difficult if there are differences in the low-level segment features. Therefore, a Generative Adversarial Network (GAN)-aided Low-Noise Discriminator (LND) is introduced to improve the denoising effectiveness in medical images with a balanced image resolution with noise mitigation. The LND function is a key that distinguishes between high- and low-noise areas based on segmented features, which are also achieved by tuning the peak signal-to-noise ratio (PSNR). Considering the training sequences, the LND-identified intervals lessen the sequences to improve the changes in pixel reconstruction. The generator function in this method is responsible for increasing the PSNR improvements over the different pixels cumulatively. The proposed method successfully improves the pixel reconstruction by 11.05% and PSNR by 9.75%, with 9.75% less reconstruction time and 13.11% less extraction error for the higher pixel distribution ratios than other contemporary methods.

Keywords: machine learning; neural networks; generative adversarial network; image denoising; medical diagnosis

JEL Classification: 68T07

Citation: Alanazi, T.M.; Mercorelli, P. Precision Denoising in Medical Imaging via Generative Adversarial Network-Aided Low-Noise Discriminator Technique. *Mathematics* **2024**, *12*, 3705. https://doi.org/10.3390/math12233705

Academic Editors: Osslan Osiris Vergara Villegas, Vianey Guadalupe Cruz Sánchez and Vicente García

Received: 6 November 2024
Revised: 22 November 2024
Accepted: 24 November 2024
Published: 26 November 2024

1. Introduction

Medical images are mostly captured via various types of scans and techniques. Medical imaging encompasses technology that provides optimal images for high-level healthcare treatments [1]. Medical image denoising is a complicated task that eliminates unwanted features from the images. A convolutional autoencoder-based denoising method is used for medical images [2]. The medical data process validates the evaluation metrics of the images, like accuracy and pixel order, and identifies the pixel that contains unnecessary noises. The unwanted noises cause complexity during diagnosis, disease detection, and ease of computation [3]. The SCAE-based method increases the accuracy of providing good medical images to further the diagnosis process. The SCAE-based method increases the accuracy of the noise reduction process [4]. Compared to traditional denoising procedures, the hierarchical feature analysis enhances pixel accuracy and preserves the imaging discrimination function [5]. An ultra-dense denoising network (UDDN) is also used for medical image denoising. The UDNN uses a feature extraction technique that extracts the essential features from the given medical images [6].

Pixel reconstruction is a process that generates medical input images from high-noise-level scanned images. Image reconstruction requires proper details, such as minimal peak signal-to-noise ratio, low mean square error (MSE), angles, pixels, and matrices of the images [7]. Pixel reconstruction is used for medical image denoising, enhancing the

diagnosis process's feasibility ratio. The noise minimization is achieved through low- and average-dose denoised image intensity measures [8]. The low-dose CT images identify the complex region that contains noise and generate alternative construction to remove the noise from the images and provide an accurate diagnosis of structure details in the image [9]. The KEM-based method increases the image reconstruction performance range, which maximizes the denoising process's reliability level [10]. An iterative denoising method using a neural network is applied for image reconstruction. The iterative method monitors the flexibility level of the images and identifies the noises [11]. The identified noises produce relevant data for image reconstruction, minimizing latency. The iterative training method improves the quality of reconstruction used for further clinical services [12].

Machine learning (ML) models are used for detection and prediction. ML algorithms are widely used for medical image denoising to enhance the precision level in the noise reduction process [13]. A deep learning (DL)-based noise suppression algorithm with adjustable weights for discrimination function, a denoising process, and a high-quality image reconstruction mechanism is used [14]. The medical image contains various unwanted noises, maximizing the complexity level in the detection and diagnosis processes [15]. The DL algorithm denoises the images and produces clear medical images, which improves the quality range of the disease detection process. A Generative Adversarial Network (GAN)-based denoising method is also used for image denoising [16]. The GAN identifies the comprehensive angle and content from the images. The identified features produce the exact noise removal region, which decreases the computational cost range during the denoising process. The GAN algorithm maximizes accuracy, improving patients' lifespans [17,18]. The challenge of traditional noise reduction methods in medical imaging lies in their inability to suppress noise and preserve fine structural features, especially when dealing with complicated distributions and varied forms of noise. To fill this need, this study introduced the GAN-aided Low-Noise Discriminator (LND), which uses a discriminator trained to zero in on areas with low-noise levels; this allows for more precise and versatile noise reduction in a range of imaging environments. In contrast to more traditional denoising techniques, this one guarantees greater retention of diagnostically significant features. Our study addresses the need for an effective and generalizable denoising model independent of modality by integrating a specialized GAN framework with noise-specific learning.

To improve noise reduction in medical imaging, the Generative Adversarial Network (GAN)-aided Low-Noise Discriminator (LND) is a deep learning-based system that has been created. It uses a GAN design, where the generator is responsible for denoising images, and the Low-Noise Discriminator improves upon it by correctly detecting and reducing patterns of residual noise. This method works well with various types of noise and different intensities; thus, it may be used for various medical imaging applications while preserving important diagnostic features.

Now, the contributions of this study are presented below:

- A discriminator function is employed for PSNR estimation to reduce noise;
- A GAN learning model is incorporated to distinguish linear and sparse distribution of pixels;
- The proposed method is validated using precision-based image reconstruction (experiments) and statistical analysis (graphical).

The rest of this study is followed by Section 2, describing a recent literature review on the proposed topic. Section 3 details the proposed Generative Adversarial Network-aided Low-Noise Discriminator method. Section 4 gives the dataset used in this study and the experimental setup. Results and discussion are given in Section 5. The conclusion is drawn in Section 6.

2. Related Works

In medical imaging, noise reduction is an important field of study since it aims to improve image clarity without losing diagnostically important features. Noise introduced

during acquisition is a common problem in medical imaging that may impact clinical decision making since it obscures crucial features and is caused by sensor limitations, patient movement, and low radiation doses. This section summarizes important research and developments in noise reduction methods applicable to this field.

2.1. Medical Image Denoising Techniques

Xu et al. [19] introduced an approach integrating secondary order-assisted total variance with deep input before picture denoising. The aim is to improve the efficiency of image denoising, and the methodology utilizes an augmented Lagrangian method to transform and effectively address the denoising challenge. The suggested technique eliminates noise while preserving intricate details.

Huang et al. [20] created low-dose CT scans that were more transparent using a better denoising method called DU-GAN with special U-Net discriminators. The goal is to boost the image quality of low-dose computed tomography (LDCT) by integrating this novel approach. The method employs a specific process to reduce radiation while ensuring accurate medical diagnoses. The technique shows excellent noise reduction, specifically for LDCT images.

Wang et al. [21] introduced a method using hybrid variation–sparse representation for more transparent medical images. The goal is to improve pictures by addressing unwanted fuzziness and distortions, enhancing overall understandability. The technique efficiently decomposes layers, handling noise, blur, and gradient loss for effective medical image enhancement. The process contributes to a comprehensive improvement in image quality by addressing various issues.

Geng et al. [22] proposed the Triplet Cross-Fusion Learning model for denoising using unpaired optical coherence-based tomography images. This approach enhances accuracy using a simpler model, requiring fewer computing resources. The method aims to improve denoising accuracy with a straightforward model structure. The technique achieves performance similar to paired methods, even with limited training data.

2.2. Refinement Techniques for Noise Reduction

Li et al. [23] introduced an innovative image-denoising method using a patch-merging refiner with UNet. The focus is on improving neutron radiography, a vital nondestructive testing technique in the industry. The approach tackles discontinuity issues in traditional threshold functions, enhancing the denoising process. The method preserves essential details in neutron radiography.

Liu et al. [24] introduced a noise estimation network for CT denoising, focusing on low dosage. The goal is to enhance denoising in low-level computer vision using a patch-merging refiner (PMR) downsample module within the CNN-UNet model. PMR uses subspace projection to eliminate noise during feature transformation while preserving authentic information. The method showcases superior anti-noise capabilities on synthetic and real-world noise images.

Liu et al. [25] introduced RA-UNet, an innovative picture-denoising model inspired by Noise2Noise. The model incorporates a multi-residual convolutional block with attention within the UNet architecture. The approach strives to improve image denoising, making generated images clearer and surpassing the denoising effectiveness of established models like DnCNN and ADNet. The method improves the extraction of crucial information, contributing to its denoising success.

Lu et al. [26] introduced a novel technique for denoising using adaptive wavelet form thresholding. The adaptive wavelet threshold mechanism contributes to the method's effectiveness in mitigating noise, showing promise for industrial image quality improvements. The technique effectively addresses Gaussian–Poisson mixed noise, a common issue in industrial testing. The method reduces the mean square error compared to four other denoising methods.

Xiao et al. [27] analyzed ACRNet for image denoising with a robust loss function. The method is based on a deep CNN, showcasing advanced ML applications. ACRNet enhances denoising by skillfully balancing receptive fields, computational simplicity, and information retention through an adaptive hierarchical structure. The method consistently provides effective denoising results across diverse tasks and image variations.

Okuwobi et al. [28] introduced an innovative method for joint denoising and augmenting multimodal medical images. The primary goal is to enhance medical image quality by integrating statistical and morphological models. The technique uses a flexible model to remove known and unknown noises in medical images. The approach improves medical image quality through a combined statistical and morphological model.

Wang et al. [29] applied MR image reconstruction using auto-encoding priors in the undecimated wavelet domain. The method uses compressive sensing to speed up magnetic resonance imaging (MRI). The technique efficiently uses MR inputs with a small sample of k-space data. The process demonstrates significant potential in enhancing the efficiency of MRI data acquisition.

2.3. Denoising Process

Guo et al. [30] improved a real-time medical image resolution using deep wavelet multiscale autonomous unmanned analysis. The goal is to enhance visual clarity by removing noise from medical images. The method is designed for real-time applications, particularly in medical image denoising and information concealment. The approach showcases the effectiveness of advanced techniques for immediate enhancements in medical imaging.

Wang et al. [31] presented a scale-sensitive GAN (ssGAN) to increase the resilience of LDCT denoising by successfully handling noise and artefacts. The suggested network has a multiscale residual discriminator that improves sample discrimination by expanding the receptive field and an error feedback pyramid generator that carries out multiscale feature extraction and noise reduction. The usefulness of this strategy for low-dose CT imaging is demonstrated by experimental results that demonstrate its superiority over current approaches in terms of structural preservation and generalization capabilities.

Chao et al. [32] improved a low-dose cone-beam CT (CBCT) using a joint denoising and interpolating network. The aim is to enhance CBCT image quality while reducing radiation exposure, making medical imaging safer. The suggested learning-based framework could be integrated into CBCT systems, advancing CBCT technology with less radiation exposure. The method achieves a milder dose reduction and improves CBCT image reconstruction.

El-Shafai et al. [33] applied different image-denoising techniques for medical images, highlighting how crucial precise noise reduction is to improve diagnostic capabilities. It discusses conventional denoising strategies and emphasizes how well deep learning methods, especially those that use convolutional neural networks (CNNs), estimate actual noise and extract pertinent features. The study also compares several approaches, outlining their benefits and drawbacks, and suggests possible medical image-based denoising research directions.

Kyung et al. [34] proposed a denoising approach, Residual Fast Fourier Transform-Aided Convolution (RFFT-Conv) blocks, with GAN enhanced by multi-task learning, for low-dose computed tomography (CT) inputs. Improved denoising performance and improved discriminator feedback are demonstrated in this research. The intricacy of putting multi-task learning into practice in clinical situations and possible difficulties generalizing the model across many CT domains are possible drawbacks.

Youyi Song et al. [35] suggested learning from AI-generated annotations for medical image segmentation. The two main concerns explored in this research are (1) the best way to quantify the loss value on AI-generated annotations, which are prone to mistakes, and (2) the best way to modify the model's parameters when the loss value is no longer an appropriate oversight for medical picture segmentation. The key takeaways are that (1) there are loss functions that can withstand mistakes and (2) when updating the model by "cross-training", which involves utilizing data from its "twin" model with a modest

loss, the model can still handle the loss function to a certain degree. The novel technique outperforms current methods for medical image segmentation when it comes to preventing annotation mistakes, according to data from a publicly accessible dataset. This opens the door to the possibility of using AI-generated annotations to train a segmentation model for medical image segmentation.

Younus FAROOQ et al. [36] proposed the Convolutional Neural Network-Based Denoising Autoencoder for Noise Removal from the Image. The suggested approach is a painstaking two-step procedure to remove background noise successfully. The first step is separating the input photos into training and testing sets. It then trains a denoising autoencoder model using the specified training data. Next, it is trained on a convolutional neural network (CNN), which improves the model's noise reduction capabilities. Data collected during testing are used to determine how well the system performs. The research uses the MATLAB R2023b programming environment for both development and testing. The suggested solution substantially outperforms the state-of-the-art methods on two separate datasets, the COVID-19 radiography database, and the SIIM medical pictures. The results were evaluated using RMSE and PSNR metrics.

Mohanapriya G et al. [37] recommended the Kalman Bucy Filtered Neuro Fuzzy Image Denoising for Medical Image Processing. The first step is to use the Kalman Bucy Filtering technique to apply measurements to medical pictures taken from the Brain MRI LGG segmentation dataset. In the second place, the membership grade addresses uncertainty in the Neutrosophic Neuro Fuzzy set (NNFS), fed filtered medical pictures as input. The three membership grades, truth, indeterminacy, and falsity, are supposed to help efficiently manage the ambiguity in noisy images. The result is a more effective image-denoising procedure with higher PSNR. Performance measures such as reduced execution time by 38% and improved PSNR and true positive rates by up to 13% and 14% are experimentally evaluated using medical images.

Karl Ludger Radke et al. [38] discussed the Chemical Exchange Saturation Transfer (CEST) magnetic resonance imaging (MRI) for denoising Synthetic Phantoms in Medical Imaging. Autoencoders were trained using synthetically produced phantoms and evaluated against classic denoising techniques on different datasets. The findings across a broad noise gamut demonstrated that NNs, especially the ResUNet designs, outperformed analytical noise detection and abatement techniques. This advantage was most apparent in the in vitro results at higher noise levels. While some conventional approaches failed, particularly in low-noise reduction cases, neural networks considerably improved PSNR values, reaching as high as 35.0.

The generalizability of existing denoising techniques for medical images is impacted by challenges with robustness over a range of noise intensities, restricted multiscale feature extraction, and high processing needs. Using an error feedback pyramid generator, the ssGAN increases sensitivity to noise at various scales while enhancing robustness and flexibility, but it still has a sparse distribution of images left unaddressed. Feature extraction is improved by a multiscale residual discriminator with a broader receptive field, guaranteeing distinct separation of the genuine signal from noise. The GAN-LND method improves LDCT denoising and achieves strong noise reduction while maintaining important image information by employing multiscale noise classification and adaptive refinement. Its sophisticated discriminator structure further enhances artefact suppression in various CT domains.

3. The Proposed Generator Discriminator-Balanced Linear Noise Discriminator Function Method

The proposed Generative Adversarial Network (GAN)-aided Low-Noise Discriminator (LND) method is designed to process the images acquired from the medical field. PSNR is extensively used in image processing research since it measures picture quality by assessing the similarity between the original and denoised images. It offers an impartial assessment of the efficacy of noise reduction while maintaining the image's structural and

textural integrity. In medical imaging, PSNR is a dependable metric for evaluating noise reduction efficacy, with higher PSNR values indicating superior retention of diagnostically significant features. The noise in the acquired image becomes difficult to reduce; at that time, the low-level segment features are disparate when tuning the PSNR, regardless of the pixel arrangement and distribution. The generator discriminator-balanced linear function is used for analyzing normal and noisy images based on the segmented features. The PSNR is computed using pixel arrangement and pixel distribution to identify the peak error. Peak error denotes the highest absolute difference between matching pixels in the original and reconstructed (denoised) pictures. This statistic is essential for assessing the worst-case scenario in picture quality deterioration, especially pertinent in medical imaging, where slight errors might influence diagnostic decisions. This ratio is aided as a quality measurement between normal and noise images, where maximum fluctuation in the input images is identified. The PSNR is measured to control noisy pixels in the input images, which are pursued using the proposed method. The mean squared error (MSE) value measures PSNR to compare image quality. The normal input image is represented as $(\mathrm{IMG}_1(r, c))$, and the compressed (reconstructed) image is represented as $(\mathrm{IMG}_2(r, c))$, processed and compared using PSNR measurement, and low-level segment features are disparate. Hence, based on pixel detection, the proposed method mainly performs two processes, including linear distribution.

Medical imaging noises, such as speckle, salt and pepper, and Gaussian, are handled well by the suggested Generative Adversarial Network (GAN)-aided Low-Noise Discriminator (LND). While the generator creates denoised images from scratch, the discriminator improves noise suppression by zeroing in on residual noise's spatial and statistical properties due to the Low-Noise Discriminator module. By capitalizing on the predictable statistical distributions and textural patterns of both speckle and Gaussian noise, the strategy outperforms previous approaches in minimizing both types of noise. On the other hand, the sparsity and irregularity of highly impulsive noises like salt and pepper make them difficult to handle. To ensure the model generalizes successfully across varied noise profiles, it is important to include adaptive training mechanisms, such as loss functions that are particular to the noise or focused augmentation procedures, to increase performance for specific types of noise.

From the diagrammatic illustration in Figure 1 below, the proposed LND method involves the following steps.

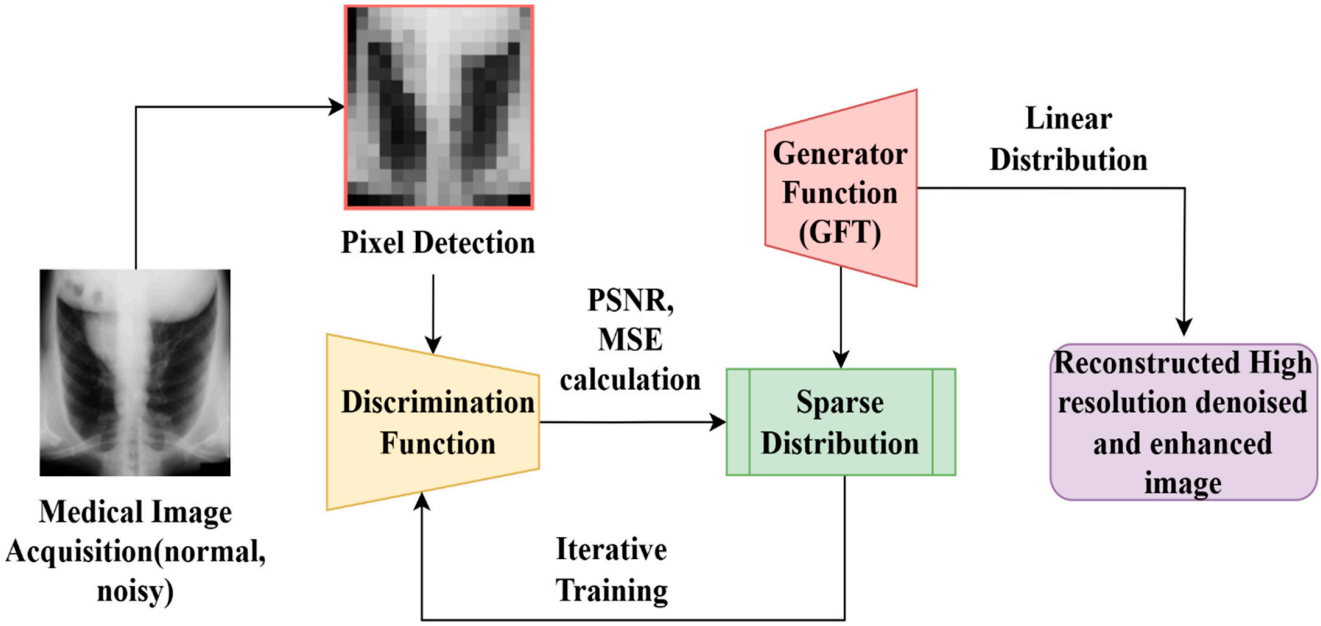

Figure 1. Graphical representation of the proposed GAN-LND method.

3.1. Pixel Detection Process

The tuning of PSNR is performed using pixel distribution and arrangement, which is responsible for denoising images from the medical field. The input features can be of any type, related to velocity, frequency, noise level, etc. Noise reduction in any type of medical image can be modelled as follows. Let us assume $M \in Rx \times x$ shows a noise image and $N \in Ry \times y$ shows the general input medical image. In this instance, the connectivity across M and N is computed as

$$M = \sigma(N) \tag{1}$$

The operation of image denoising of a noisy input is to identify a discrimination function termed Df to satisfy

$$\underset{Df}{\operatorname{argmin}} \|N - Df(M)\|^2 \tag{2}$$

This proposed method aims to find an alternate discrimination function Df to maximize PSNR. This process maps the normal and noisy images to improve the discrimination function. Low-Noise Discrimination functions with low-level segmented features can solve the precise pixel distribution. Hence, the MSE computed for the acquired image is as follows.

$$MSE = \frac{\sum_{r,c}[((IMG_1(r,c)) - (IMG_2(r,c)))]^2}{M \times N} + (Df_{max} - Df_{min}) \tag{3}$$

where the variables r and c are used to represent the row and column of the medical images. Therefore, the MSE value via PSNR is computed as follows:

$$PSNR = 20\log_{20}\left(\frac{\left(\max\limits_{0\le x,y\le 1} Fe^{-x,y^2}\right)^2}{MSE}\right) \tag{4}$$

Equation (4) shows PSNR is derived from its definition as a logarithmic measure of the ratio between the maximum possible power of a signal (the image's maximum fluctuation) and the power of the noise (MSE). In Equation (4), the variables F and e represent the input medical image's maximum fluctuation (variation) and pixel error. Using these features, the process of detecting the pixels is performed as follows:

$$Pixel_d = \frac{1}{\sqrt{M * N}}\left[\frac{\left(\frac{\max\limits_{0\le x,y\le 1} Fe^{-x,y^2}}{\min\limits_{0\le x,y\le 1} Fe^{-x,y^2}} - \frac{M(r,c)}{N(r,c)}\right)}{2(N - Df(M))}\right] \tag{5}$$

Equation (5) expands upon the pixel-level error detection by considering the normalized fluctuation range of pixel intensities, represented by F, relative to the minimum and maximum intensities observed in the noisy image, where $\frac{M(r,c)}{N(r,c)}$ are the current noise-contaminated version of the image and its corresponding raw input. The conditions $\max\limits_{0\le x,y\le 1} Fe^{-x,y^2}$ and $\min\limits_{0\le x,y\le 1} Fe^{-x,y^2}$ represent the maximum possible fluctuation and error pixel and the minimum possible fluctuation and error pixel observed from the input images. The variables ϑ, frq and $\exists$ are used to represent the velocity, frequency, and discolouration observed in both the raw and noise images. This observation is used to compare the images for suppressing the noise present in the images. The pixel distribution process is illustrated in Figure 2. The main goal of the proposed GAN-aided Low-Noise Discriminator (LND) approach is to learn and reduce noise patterns that are shared across several imaging modalities, making it technology agnostic. These modalities include CT, MRI, and X-rays. The

model was trained to generalize across varied acquisition settings by exposing it to a wide dataset that included images from several imaging modalities with differing noise characteristics. The level of artefacts or noise elements that are distinctive to a certain modality may cause it to function differently. Examining the possibility of combining modality-focused pretraining with domain-specific fine-tuning might increase generalizability.

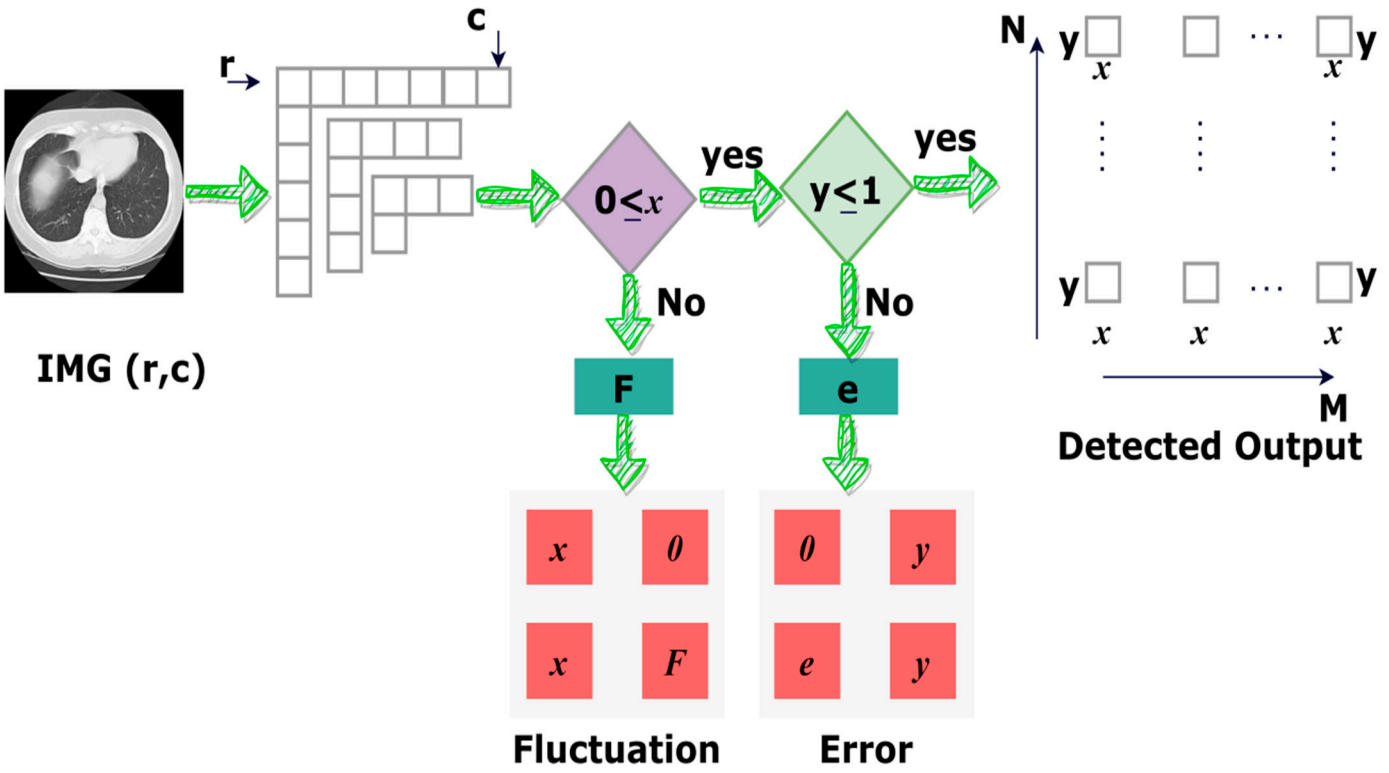

Figure 2. Pixel_d detection from $\text{M} \in \text{Rx} \times \text{x}$.

$\text{IMG}_1(\text{r}, \text{c})$ is the input that is first discriminated as $(\text{r} * \text{c})$ to extract PSNR from each of its distributions. Two conditions, $0 \leq \text{x}$ and $\text{y} \leq 1$, are, respectively, validated for F and e presence, such that the distribution is found. This distribution is validated for $(\text{x} * \text{x}) \in \text{M}$ and $(\text{y} * \text{y}) \in \text{N}$ until the maximum discrimination to the last pixel is detected. The pixel_d is, thus, the output of $(\text{M} * \text{N}) \forall (\text{x} * \text{y})$ identified with Df (Figure 2). For the different Pixel_d, the extraction rate is specified in Table 1. This rate is presented from the dataset images accounted for in this study. Pixel intensity changes and noise patterns are the main targets of the proposed technique. These aspects are crucial for medical images and diagnostic accuracy. Image transparency and shadow rate are crucial features, yet they usually come into their own when dealing with certain imaging modalities or sophisticated visualization methods. With a focus on noise reduction and structural preservation, our current model is built to generalize across various medical images.

Table 1. Pixel_d for different $(\text{r} * \text{c})$.

r×c	PSNR	F	e	Pixel_d
1×1	26.3	± 0.11	0.42	0.59
2×2	28.6	± 0.101	0.38	0.72
4×4	31.25	± 0.008	-0.07	0.85
8×8	29.25	± 0.101	-0.02	0.92
16×16	32.2	± 0.086	-0.08	0.91
32×32	35.04	± 0.095	-0.09	0.9
64×64	28.69	± 0.105	0.12	0.65
128×128	35.07	± 0.07	-0.085	0.85

The above tabulation is presented for a single IMG, (r, c) fetched from the dataset. The $(r \times c)$ is varied between (1×1) and (128×128) for the size and texture used for diagnosis. In this process, the Df determines F for the achievable PDNR. As the F variates, the e is influenced throughout, such that Pixel_d is impacted. Considering the difference between successive $(r \times c)$ utilized F, the e is computed. Therefore, the reconstruction process sustains this flaw using GAN, which will be discussed later (Table 1).

3.2. Low-Discrimination Function

The velocity, frequency, and discoloration are computed as the number of noisy pixels detected in different regions. In such cases, the error causes pixels to take place in $N(r, c)$ due to noise occurrence. Equation (6) defines the low-discrimination function, Low(Df), as a measure of how noise impacts pixel intensity distribution. Therefore, these noises present in an input image impact the available networks in any instance for which the low-discrimination function is performed, as follows

$$\text{Low}(\text{Df}) = \frac{\vartheta + \text{frq} + \exists}{\left(\frac{\max\limits_{0 \le x,y \le 1} \text{Fe}^{-x,y^2}}{\min\limits_{0 \le x,y \le 1} \text{Fe}^{-x,y^2}} - \sigma \right)^2} \tag{6}$$

In this medical image processing, the PSNR is used to identify noise presence in an input image and find the noise properties in a particular region with a discrimination function. We identify the noise presence in the spatial domain because it is easy to define and classify the smooth and noisy pixels in a specific region. If a region containing low-level segment features is selected and the presence of noisy pixels is suppressed using GAN-aided LND, the variations in the selected region are due to the noisy pixel distribution. Moreover, the chosen smooth region was independently analyzed to overcome the impact of non-smooth regions. Hence, it is the best way to estimate noise.

3.3. Mean Deviation and Standard Deviation Calculation

We can validate the mean deviation rather than the standard deviation to compute the noisy pixel distribution. In this proposed method, the mean deviation is more efficient than the standard deviation considering the metrics. The standard deviation leads to improper noise validation. Therefore, we can use the mean deviation value for precise noise estimation. The mean deviation is represented as Δ the difference between pixel values $\alpha(x, y)$, and their mean μ_{mean} is expressed as

$$\Delta = \frac{1}{MN} \sum_{x=1}^{M} \sum_{y=1}^{N} \| \alpha(x, y) - \mu_{\text{mean}} \|^2 \tag{7}$$

where

$$\mu_{\text{mean}} = \frac{1}{MN} \sum_{x=1}^{M} \sum_{y=1}^{N} \alpha(x, y) \tag{8}$$

where Δ represents the mean difference or absolute mean deviation observed in the pixels. Contrarily, the standard deviation σ is estimated as

$$\sigma = \sqrt{\frac{1}{MN} \sum_{x=1}^{M} \sum_{y=1}^{N} (\alpha(x, y) - \mu_{\text{mean}})^2} \tag{9}$$

In Equation (9), the pixel detection in an input image contains the mean deviation Δ and the standard deviation σ due to unnecessary noisy pixels in images. Here, this deviation is computed to overcome the issues for which the appropriate pixel reconstruction is made. The discriminator function definition is presented in Algorithm 1.

Algorithm 1: Discriminator Function Definition

Input $DF(Pixel_d, r, c)$
Output low MSE

1. Initialize $r \in \{1, 2, \ldots, x\}, c \in \{1, 2, \ldots, y\}$
2. calculate Df as $M = o(N)$ such that $\text{argmin}||N - Df(M)||^2$

if $Df(\text{pixel}) = \max_{0<x}$ then
calculate $\mu = a(x, y) \cdot \frac{1}{r \times c}$
calculate $\frac{\vartheta + frq + \exists}{\left(\frac{\max_{0 \le x,y \le 1} Fe^{-x,y^2}}{\min_{0 \le x,y \le 1} Fe^{-x,y^2}} - \sigma \right)^2}$
else if $Df(\text{pixel}) = \min_{0<y}$ then
$F = \max_{0<x} - c$
$r = \frac{F}{y}$
$Df = \text{high}$
end if

3. calculate μ_{mean} where $(M * N) \forall (x * y)$
4. calculate MSE

3.4. Generative Adversarial Network Architecture

The low-resolution image is processed to convert into a high-resolution image to achieve super-resolution for improving medical diagnosis. GAN is an essential tool for performing image denoising. Generally, GAN performs two functions: discrimination function DFT and generator function GFT. In this study, the generator function increases the PSNR across various pixels, whereas the discriminator function suppresses the pixel noise and maximizes PSNR. This generator function generates artificial sample images based on original pixel values from low-level segmented features. Utilizing 3×3 kernel sizes, ReLU activations, and skip connections to maintain spatial information, the generator architecture comprises convolutional layers with residual blocks intended to capture complex noise patterns and recreate medical pictures devoid of noise. For hierarchical analysis of noisy features, the discriminator uses convolutional layers with progressively larger filter sizes (e.g., 64, 128, 256), batch normalization, and LeakyReLU activations to improve feature learning and stability. The LND module also incorporates an auxiliary classifier that focuses on separating areas with high and low noise to improve pixel and perceptual accuracy. This classifier makes use of a hybrid loss function. The Df in the PSNR measurement is used to classify the original sample and artificial sample image. The generator function is used to camouflage the Low-Noise Discriminator using optimization with pixel distribution. From the process, a Low-Noise Discrimination function is trained to maximize PSNR. Considering the training sequences, the low-discrimination function identified that intervals are reduced to increase the swiftness in denoising (pixel reconstruction). Therefore, the process of GAN is as follows: if the generator function produces a sample, then a high-noise discriminator function is observed, which proves that the generator function is trained well and that the discriminator network can easily distinguish between the linear distribution and sparse distribution. Therefore, the effect of the generator function is insufficient for further processes. This pair of discriminator and generator functions is trained alternatively until the PSNR is increased. Therefore, the PSNR is computed as linear distributions without sparse distributions influenced by noisy pixels. Mathematically, GAN contains the generator and discriminator function with min/max condition formulated as

$$\min_{DFT} \max_{GFT} L_d[\log((DFT(x, y)))] + Sp_d[\log(1 - (DFT(GFT(n))))] \quad (10)$$

where L_d and Sp_d are the linear and sparse distribution of raw and compressed images observed from the input images, respectively. The variable $(DFT(x, y))$ represents the probability of x and y subjected to the original image pixels, and n is the noise in the

acquired images. Image denoising is processed to enhance the quality of such images by suppressing the noise. In this scenario, the x and y wavelet-based method is used to achieve the best denoising method. The GAN for (x, y) until (M, N) is illustrated in Figure 3.

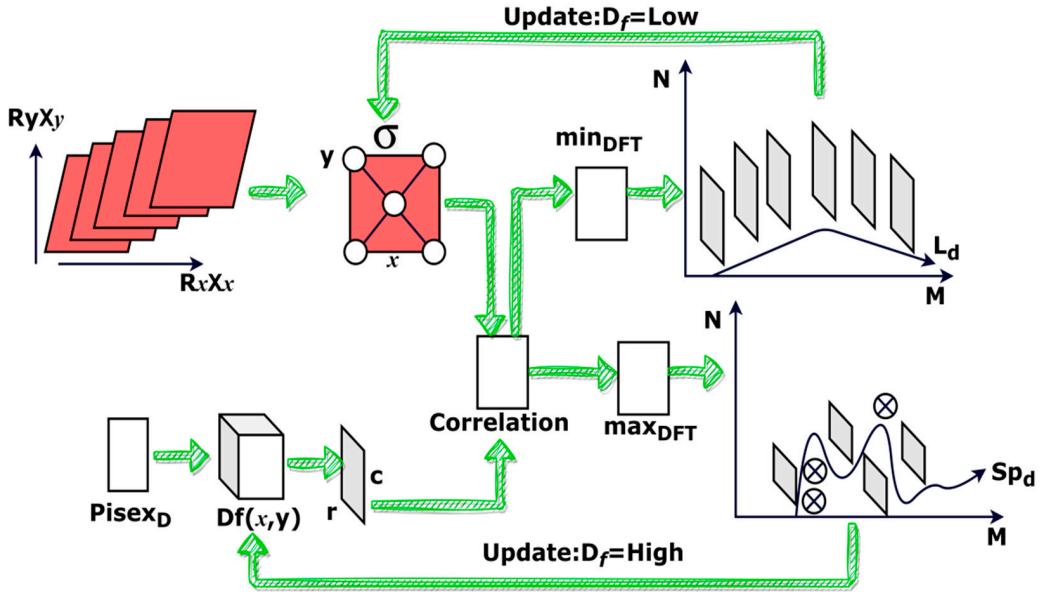

Figure 3. GAN representation for L_d and Sp_d for (x, y) until (M, N).

Image quality can be drastically reduced when the discriminator incorrectly identifies low-noise regions as high-noise ones or vice versa. A loss of important diagnostic features might occur due to over-smoothing caused by false positives, which make low-noise areas noisy. Alternatively, medical imaging features like tiny lesions or tissue textures might be obscured by residual noise caused by false negatives, which fail to identify high-noise locations. By making it harder to see important structures, these mistakes directly impact diagnostic accuracy and may cause misunderstandings or forgotten diagnoses. The suggested GAN-assisted Low-Noise Discriminator (LND) uses adaptive loss functions and robust training to reduce the risks of misclassifications. Using a carefully selected dataset with a wide range of noise levels and patterns, the discriminator is trained to correctly distinguish between various kinds of noise and their intensities. To further reduce the number of false positives and negatives, the discriminator incorporates a hybrid loss function that considers feature-level realism alongside pixel-wise accuracy. Correcting training-stage misclassifications and improving the model's capacity to retain critical diagnostic features are achieved by iterative feedback between the discriminator and generator, further refining the noise removal process.

In Figure 3 above, the GAN representation for $[(Ry \times y)(Rx \times x)]$ and $Df(x, y)$ until $(M \times N)$ is given. In this process, the generator function is responsible for the correlation of $\sigma(x, y)$ with $Df(x = r, y = c)$ in $pixel_d$. The outputs (succeeding) in min_{DFT} and (failing)max_{GFT} are used to detect L_d and S_{pd} for the matching $(M \times N)Pixel_d$. Therefore, the discriminator σ and generator μ_{mean} are trained using L_d and S_{pd} under consecutive pixel distributions (Figure 3). Based on the increasing network depth, the segment features in each layer rely on various fields. In this scenario, the proposed Generative Adversarial Network-aided LND is applied to obtain complete data and connectivity in each layer. In this research, pixel reconstruction improves the medical image resolution and reduces noisy pixels. To improve the PSNR in each pixel distribution, pixel reconstruction is utilized for the generator function. In this research, the GAN-LND with identified intervals is handled to extract the sequences from each pixel. This way, the PSNR is computed as linear distributions without sparse distributions influenced by noise pixels; the extractable sequences are used for diagnosis. From the above GAN representation, the different L_d and Sp_d rates for several iterations are tabulated in Table 2.

Table 2. L_d and Sp_d for several iterations and r × c.

r×c	Iterations	L_d	Sp_d	Correlation Factor
2 × 2	300	−0.27	−0.38	0.52
	1200	0.12	0.32	0.72
4 × 4	300	−0.101	0.37	0.62
	1200	0.25	0.25	0.78
8 × 8	300	0.18	−0.101	0.56
	1200	0.31	0.52	0.82
16 × 16	300	0.32	−0.21	0.71
	1200	0.425	0.48	0.88
32 × 32	300	0.32	0.23	0.75
	1200	0.44	0.51	0.85

In Table 2, the L_d and Sp_d for $(r \times c)$ fewer than 1200 training iterations with the correlation factor are presented. L_d and sp_d are inversely proportional based on the available v, frq, and $\exists$. As the $\exists$ correlation increases, it decreases to under-distinguishable Δ. Therefore, $low(Df)$ is the accidental case that validates (x, y) with (r, c) until (M, N). The $\beta(x, y)$ requires high (stabilized) L_d to improve image quality and free it from noise. This feature alone increases the PSNR of the $IMG_2(r, c)$ by augmenting min_{DFT}.

3.5. Loss Function

The loss function is challenging to define for the GAN-aided LND-aided image denoising process. The loss function of sparse distribution impacts the noisy pixels for precise image restoration. The various medical image denoising processes are employed for different loss functions. The MSE or $Loss_f$ is the primarily used GAN-based method to increase PSNR. However, this method includes the sparse distribution, which causes log loss and cross-entropy loss. Furthermore, in this study, we estimate the PSNR measurement with loss. To effectively deal with different types of noisy images, the structural loss $P_\theta(x_0, y_0)$ is identified from the $Loss_f$. Hence, the final $Loss_f$ is computed as

$$P_\theta(x_0, y_0) = \int P_\theta\left(x_{0_t}, y_{0_t}\right) dx_t \tag{11}$$

and

$$Loss_f = -\log\left(P_\theta(x_0, y_0)\right) \tag{12}$$

The above equation follows the linear and sparse distribution from the extractable sequence until the noisy pixels from such images are categorized. The current input image is handled to reduce noisy pixel occurrence depending on the LND-identified intervals until swiftness in pixel reconstruction is improved. The above sequence of LND-identified intervals is analyzed using the linear distribution output to reduce noise between the same pixels. In this scenario, the observed data from input medical images must be converted into controls to be distributed for accurate LND-identified time intervals to increase PSNR measurement. In addition, the linear pixel distribution is instantaneous to meet the high-level segment features using the discriminator function. Therefore, the generator and discriminator functions are used to measure PSNR for pixel reconstruction. In Algorithm 2, the $Loss_f$ description is presented. Reconstruction accuracy may be easily measured by minimizing the mean square error (MSE) and quantifying the pixel-wise differences between the original and rebuilt images. Low mean square error is considered very important in image reconstruction. Reconstructing images with a low mean squared error (MSE) ensures that diagnostically significant information is maintained, which is crucial in medical imaging.

Algorithm 2: Loss Function Loss_f Description

Input $P_\theta(x_0, y_0)$
Output Loss_f computed loss for the GAN-based image denoising

5. Initialize $\text{Loss}_f = 0, \min_{DFT}, \max_{GFT}, n$
6. for each noisy pixel in the image, do
   a. identify pixel(x, y)
   b. calculate reconstruction loss

$P_\theta(x_0, y_0) = \int P_\theta\left(x_{0_t}, y_{0_t}\right) dx_t$
if $\{F > P_\theta(x_0, y_0)\}$ then
update $\text{Loss}_f = -\log((P_\theta(x_0, y_0)), +\log(P_\theta(r, c)))$
$P_\theta(x_0, y_0) = dx_t + dy_t$
else if $\{F \leq P_\theta(x_0, y_0)\}$ then
$\text{Loss}_f = -\log(P_\theta(x_0, y_0))$
$P_\theta(x_0, y_0) = dx_t \text{or} dy_t$
end if

7. calculate $\frac{\sum_{r,c}[((IMG_1(r,c)) - (IMG_2(r,c)))]^2}{M \times N} + (Df_{max} - Df_{min})$
8. $\text{Total}_{loss} = \text{Loss}_f + \text{Loss}_{GAN}$

3.6. Image Reconstruction Process

The GAN output identifies and differentiates the linear and sparse distribution in this image reconstruction process. The training is performed through PSNR measurement and extractable sequences to satisfy the Low-Discrimination function. The first step of this discriminator function is to sample the accurate noisy pixel detection sequences if the loss function is computed. The generator function satisfies the maximum PSNR measurement over the different pixels, which is the best output for performing high-pixel reconstruction. The serving inputs for the training are the extractable sequence from sparse distribution, the consecutive samples of 00, 01, 10, and 11 across the different pixels at different time intervals. For increasing the PSNR measurement, the assessment initiates from the extractable sequences with the first training set as $IMG_1(r, c)$. This training is the sparse distribution-observed instance. The noisy pixel is identified if this distribution is observed in any sequence (later). Hence, in the GAN-based method, the sparse distribution is accounted for when identifying the noisy pixels in input images. In this study, the noisy pixel detected image and its corresponding image are processed for similarity analysis, and this analysis output is inputted to the network to improve PSNR. In this way, the pixel distribution is enhanced to improve reconstruction. Additionally, this study employed linear distribution without sparse distribution, suppressing the reconstruction and loss function to train the extractable sequences for satisfying the low-discrimination function. The input image has been compressed for rows and columns, and the raw image is required through various methods. GAN-based LND-identified intervals represent a better reconstruction output than other methods. However, the reconstruction reduces noisy pixels from the acquired images between similar pixels based on training the GAN function using a linear distribution output. This problem is overcome using the proposed method and discriminator function. Based on GAN-aided LND, the additional method to estimate the difference between the denoised and ground-truth images is to mitigate the network convergence and sparse distributions. The image reconstruction process is illustrated in Figure 4.

The $\min_{DFT} \cdot \max_{GFT}$ is the actual reconstructed output with Loss_f. The $DFT_{x,y}$ is required for L_d and Sp_d differentiation for $(r \times c)$ across $P_\theta(x_o, y_o)$. If the matching criteria satisfy $\max_{o<x}$ and $\min_{y \leq 1}$, then $P_\theta(x_o, y_o)$, the reconstruction is performed using dx_t and dy_t. Therefore the Δ is the non-replaceable pixel regions of $L_d \cap Sp_d$, for which reconstruction is performed (Figure 4). Image Reconstruction using GAN is given in Algorithm 3.

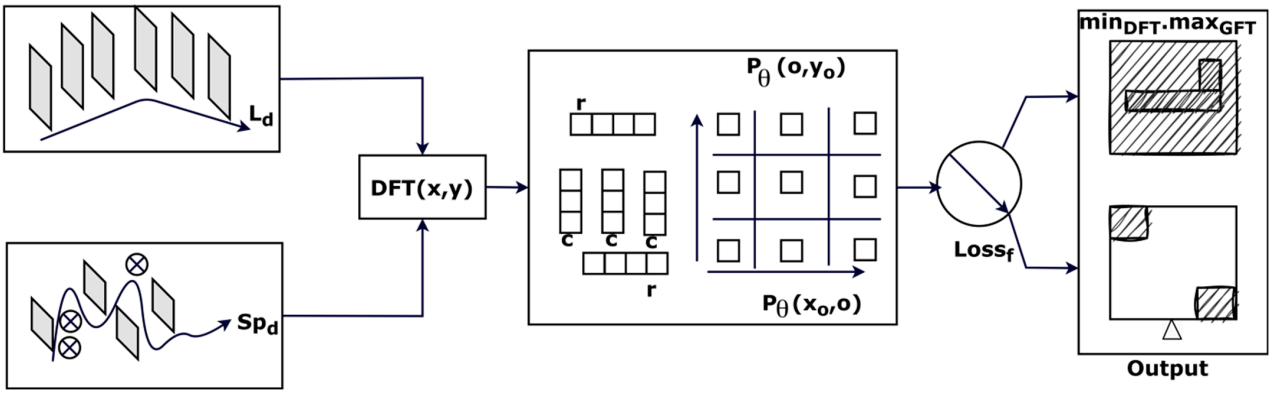

Figure 4. Image reconstruction process using (x_0, y_0).

Algorithm 3: Image Reconstruction using GAN

Input $IMG_1(r, c)$
Output $IMG_{reconstructed}(r, c)$, PSNR

1. Initialize GAN G, D
2. for each iteration, do
   a. sample noisy pixels from IMG_1
   b. calculate $P_\theta\left(x_{0_t}, y_{0_t}\right) = G_{noisy}$
   c. compute $Loss_f = -\log\left(\left(P_\theta\left(x_0, y_0\right)\right)\right)$
   d. update G and D using $Loss_f$
3. denoise $IMG_{reconstructed}(r, c) = G(IMG_1)$
4. Calculate PSNR between $IMG_{reconstructed}(r, c)$ and $\min_{DFT} \cdot \max_{GFT}$
5. return $P_\theta\left(x_o, y_o\right)$

In the proposed network, the final reconstruction loss is defined as

$$\min_{DFT} \max_{GFT} Loss_f(DFT(x, y), GFT(x, y)) + \beta_{loss}(GFT(x, y)) \quad (13)$$

Based on the initial and extractable sequences, the linear distribution output is used to train the GAN function. In the first extraction, the discriminator function is defined to improve the pixel reconstruction, and, therefore, PSNR measurement is the output for the other parameters. Hence, the precise tuning of PSNR is performed to improve image quality without sparse distribution. Instead, the case of extractable sequences varies for each pixel, affecting the training set. Based on the linear distribution output, the noise is suppressed.

4. Dataset and Experimental Setup

The Discussion section is presented in two segments: experimental analysis and comparative study. The medical noisy images from (http://imgcom.jsrt.or.jp/minijsrtdb/, accessed on 5 October 2024) are used in the experimental analysis. This image source provides 244 images in 4 orientations, making it 988 in count. The number of images used in testing is 10, which shows up in 2×2, 4×4, 8×8, and 16×16 pixel distribution sizes. The images are related to thorax mass shadow using radiology observations. The GAN layers are trained for 1200 iterations to verify and validate the input image for precision. Therefore, the different input sizes are analyzed in Table 3.

Apart from the above experimental analysis, the following metrics, pixel reconstruction, PSNR, noise estimation, reconstruction time, and extraction time, are analyzed. This analysis is presented as a comparative discussion with the existing WDAEP [29], DU-GAN [20], and SWM-DE [28] methods. As discussed, the X variants are the training sequences (100 to 1200) and the pixel distribution rate (0.05 to 0.8).

Table 3. Experimental result analysis.

Sample Input	F	L_d	Sp_d	$(DFT(x,y),GFT(x,y))$
				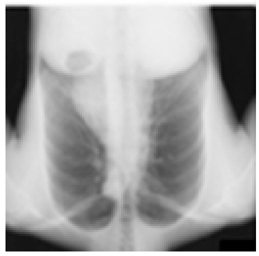
				
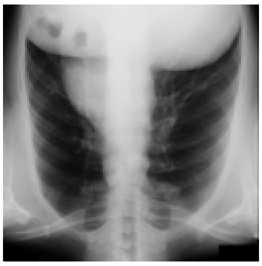	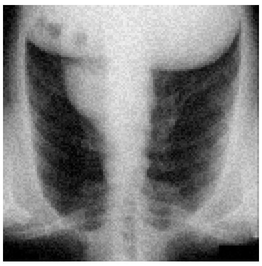		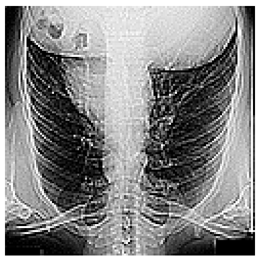	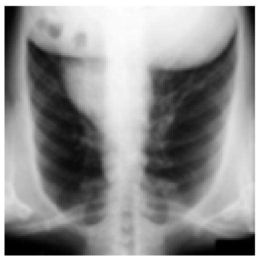
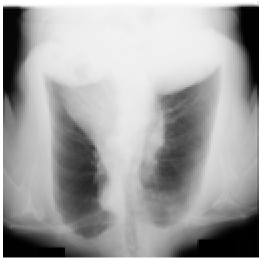	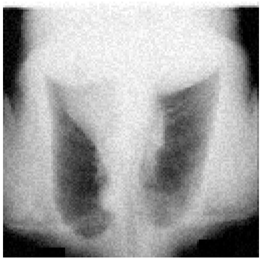		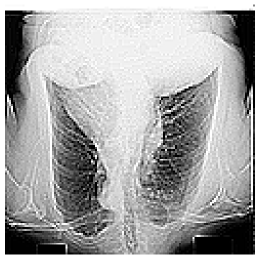	

5. Results and Discussion

5.1. Pixel Reconstruction

In this proposed method, the GAN-based PSNR estimation is performed through a low-discrimination function for improving pixel reconstruction and distribution based on noisy pixel occurrence (refer to Figure 5).

The linear distribution without sparse distribution is influenced by noisy pixels based on the extractable sequences for diagnosis. The similarity analysis between each layer's raw and noisy images is processed to satisfy high pixel reconstruction. The identified LND intervals from generator and discriminator functions are mitigated using linear distribution to improve PSNR. The low-level segment features obtained from the acquired medical images are sequentially analyzed to achieve maximum noise estimation and PSNR measurement with less loss and reconstruction time. The extractable sequence of the GAN function is trained alone using the linear distribution output to identify noisy pixels. The proposed method addresses the extraction error and reduces improper disease diagnosis. This extraction achieves high-noise estimation for accurate and appropriate pixel distribution. The losses are confined to the proposed method for achieving high-pixel reconstruction.

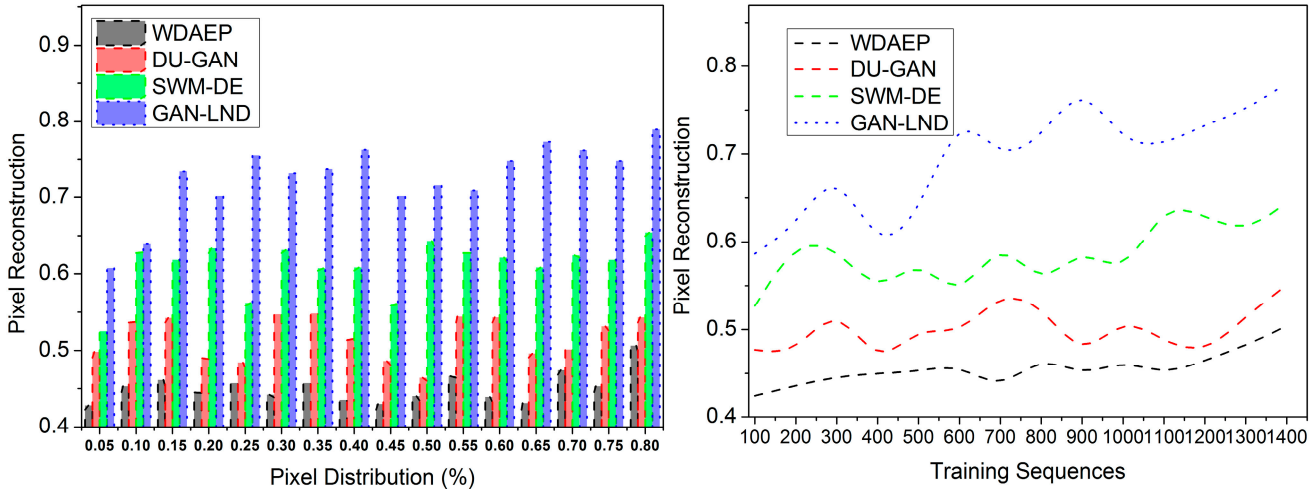

Figure 5. Pixel reconstruction.

5.2. PSNR Analysis

This proposed method uses the GAN function to satisfy high-PSNR measurements concerning the generator and discriminator network across different layers in different time intervals (refer to Figure 6). The high/low-discrimination functions are identified using linear distribution to improve PSNR from the extractable sequences. Based on the training sequences, the generator network generates better output images from high-resolution images to prevent noisy pixels. In this manuscript, the GAN function is trained to create better images and improve PSNR measurement without sparse distribution. The GAN-aided LND is applied to obtain better image representation and improve diagnosis. GAN is used to observe low-radiation-dose medical images and perform denoising to generate noise-less medical images. This noisy pixel is detected from such images; GAN is applied to consider the training sequences for improving PSNR measurement. In the sequential training of the GAN function, the LND-detected intervals are reduced from the sequences. Therefore, this study achieves a high PSNR.

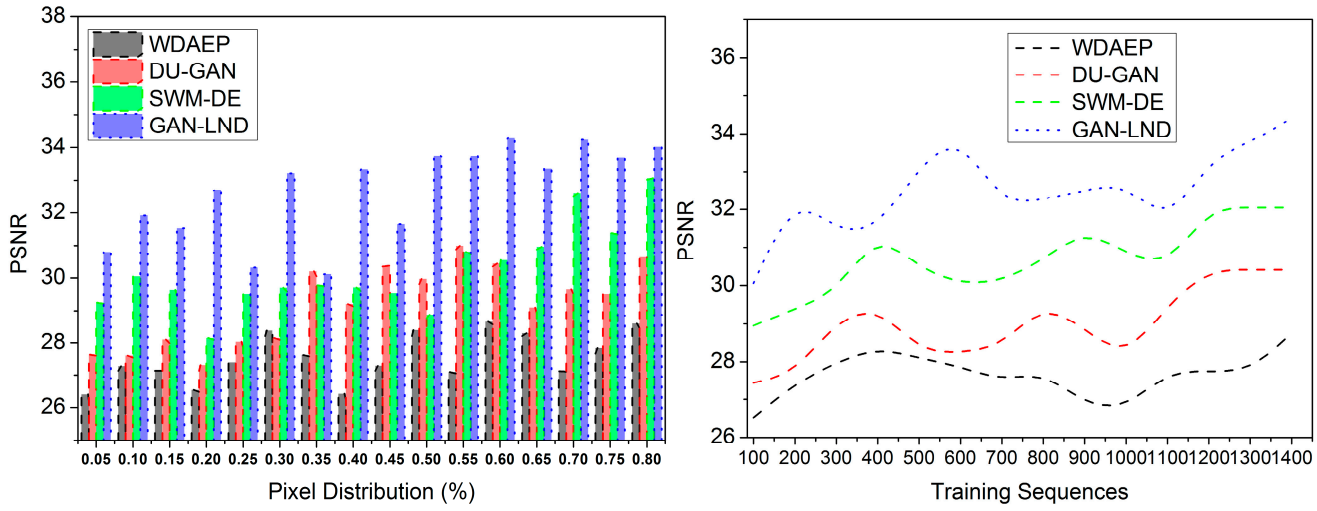

Figure 6. PSNR.

5.3. Noise Estimation

In this study, the proposed method using the linear distribution of pixels to improve the visual image quality and its representation for addressing the low-noise discriminator identified at different intervals is to satisfy high-noise satisfaction (refer to Figure 7). Considering training sequences based on the acquired medical images' pixel distribution, the noisy

pixels are reduced to generate high-resolution images to improve PSNR. The considerable segment features fluctuate concerning the discrimination function for maximizing PSNR. Therefore, extraction errors are identified by comparing the quality of the processed images with the original images to prevent noise. Based on the low-discriminator function, the noise of pixels is reduced to maximize noise estimation. The proposed method first detects the pixels to preserve the structural information and then verifies pixel reconstruction to minimize the Low-Noise Discriminator from the sequence. In this image denoising process, the standard and noisy images are compared to classify the high/low segment features for pixel detection to reduce losses at different intervals.

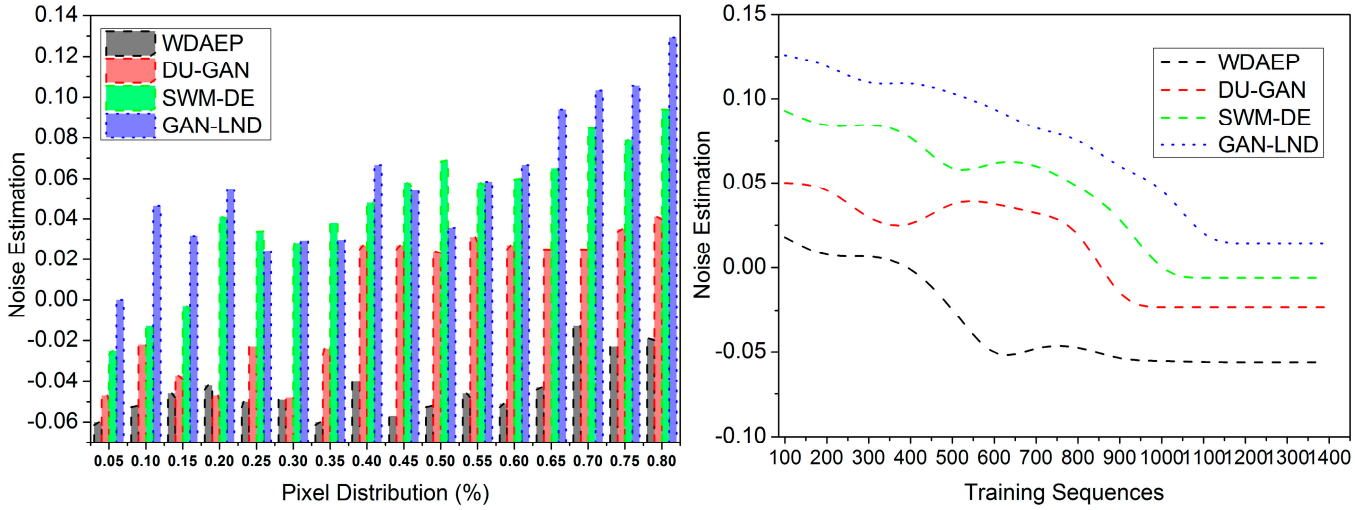

Figure 7. Noise estimation.

5.4. Reconstruction Time

In this proposed method, high-pixel detection and noise estimation are performed for the GAN function in each layer for better pixel reconstruction to reduce reconstruction time (refer to Figure 8). The generator and discriminator network are balanced using linear distribution for comparing ground-truth images and noisy images based on the segmented features levels. The PSNR measurement is computed using the GAN function to identify the errors. The quality measurement may differ for each pixel for varying pixel features to satisfy high-noise estimation; the proposed method is used to modify the discrimination function for maximizing PSNR measurement. This method compares the original and noisy images to improve pixel reconstruction and generate a new image. In this study, the training of the GAN function is performed until high-noise discrimination; this instance is terminated to prevent extraction errors. In this scenario, the accurate pixel distribution is solved based on the Low-Noise Discrimination functions with low-level segmented features to reduce the swiftness in pixel reconstruction. Hence, the proposed method will satisfy the reconstruction in a timeless manner.

5.5. Extraction Error

This proposed method aided in achieving high-resolution images without sparse distribution, which is the better output for generating new clear images. In this scenario, the pixel detection has less extraction error and reconstruction time than the other factors, as represented in Figure 9.

The conditions of $\max_{0\leq x,y\leq 1} Fe^{-x,y^2}$ and $\min_{0\leq x,y\leq 1} Fe^{-x,y^2}$ show the maximum possible fluctuation and error pixel and minimum possible fluctuation and error pixel observed from the input images for maximizing PSNR. This PSNR measurement is used to identify the difference between the original and ground-truth images to suppress the noise occurrence in the images. In such cases, the extraction error in $N(r, c)$ is due to noise occurrence, which

is identified using the generator function. We can perform denoising based on the generator discriminator-balanced linear function to improve pixel reconstruction. The generator function notices the extraction errors from the acquired images to reduce reconstruction time. Therefore, the noise of pixels changes based on the discriminator and generator function, and a high medical diagnosis is achievable. Therefore, the proposed method reduces extraction errors. Apart from the above comparative analysis, the impact of the methods on different distributions for the $(\mathrm{DFT}(x, y), \mathrm{GFT}(x, y))$ is validated in Table 4.

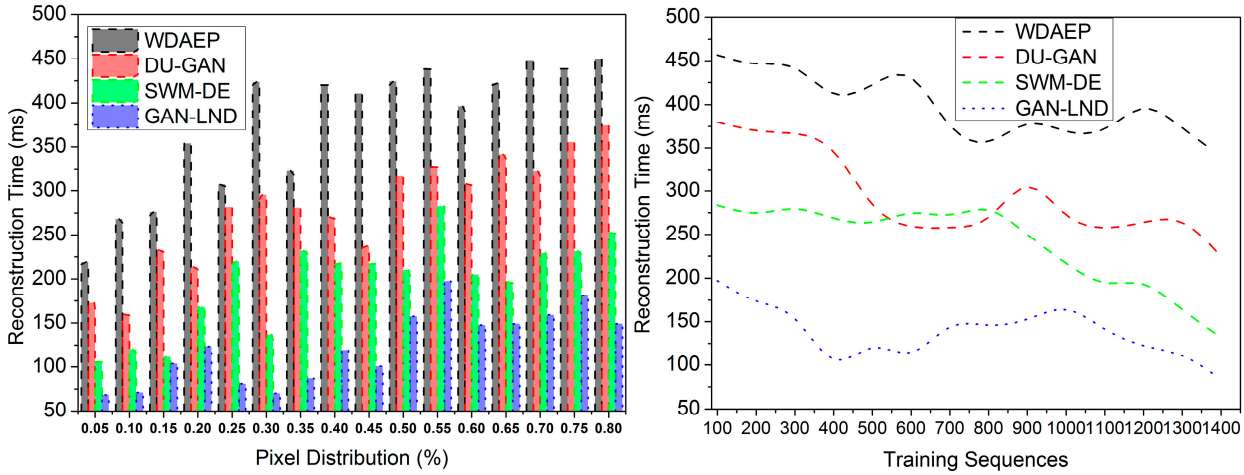

Figure 8. Reconstruction time.

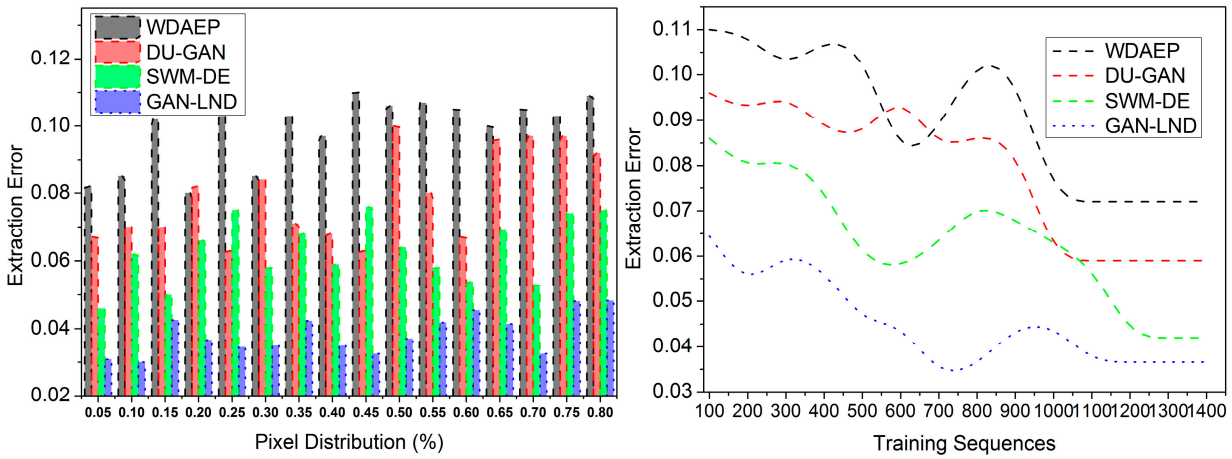

Figure 9. Extraction error.

Table 4. $(\mathrm{DFT}(x, y), \mathrm{GFT}(x, y))$ for different methods.

Methods	r×c	$P_\theta(x_0, y_0)$	(DFT(x,y),GFT(x,y))
WDAEP	2 × 2	6.25	0.62
	4 × 4	0.42	0.52
	8 × 8	0.13	0.42
DU-GAN	2 × 2	7.45	0.521
	4 × 4	4.52	0.658
	8 × 8	3.25	0.596
SWM-DE	2 × 2	8.69	0.636
	4 × 4	7.25	0.425
	8 × 8	6.321	0.525
GAN-LND	**2×2**	**8.45**	**0.63**
	4×4	**9.65**	**0.65**
	8×8	**10.05**	**0.79**

The above tabulation is the signified inclusion of different methods and their impact on different $Pixel_d$. The standard deviation and error factors are estimated based on their operational principle and learning. Therefore, the persistent outputs under L_d and Sp_d are identified and cumulatively summarized as the reconstruction possibilities in Table 4 above.

6. Conclusions

This study described a Generative Adversarial Network-aided Low-Noise Discriminator. The GAN-aided LND is proposed to reduce the noise of pixels using a low-discrimination function to maximize the PSNR. The GAN is used in medical image denoising with observed features from different scanning/input devices. The noisy pixels are detected from any images using GAN training sequence considerations. In the sequential training of noisy input images, the LND-detected intervals are reduced from the sequences. This process leads to high-pixel reconstruction. In particular, the pixel reconstruction relies on the distribution and least possible noise pixel extractions. The LND-identified intervals improve the training for sparse and linear distributions. The conjugated output between the distributions is induced with a loss function that retains noiseless pixels, and the same function is used for image reconstruction. This improves the pixel reconstruction by 11.05% and PSNR by 9.75%, with 9.75% less reconstruction time and 13.11% less extraction error for the higher pixel distribution ratios.

The noise features in medical imaging might differ significantly within and between images. However, input images with several noise sources or complicated noise distributions could negatively impact the GAN-aided LND's efforts. Medical imaging noise features are famously complicated and variable, a major obstacle for the GAN-aided LND method. Variations in acquisition environments, hardware inconsistencies, and patient-specific features may cause noise characteristics to vary greatly among and even within imaging modalities (e.g., X-rays, CT, and MRI). These modifications test the model's generalizability, especially for input images with several noise sources or non-Gaussian distributions with non-normal patterns. Artefacts or inadequate noise reduction in certain areas may result if the discriminator cannot properly distinguish high-noise regions in such a scenario. Developing the GAN model training on cross-modal noise mitigation using data from different types of medical imaging (e.g., X-ray, CT, and MRI) will be examined in a future study to increase reconstruction quality and its capacity to generalize to varied medical situations.

Author Contributions: Conceptualization, T.M.A. and P.M.; Methodology, T.M.A.; Writing—original draft, T.M.A. and P.M.; Writing—review & editing, P.M.; Supervision, P.M.; Project administration, P.M. All authors have read and agreed to the published version of the manuscript.

Funding: This research received no external funding.

Data Availability Statement: The data will be made available by the authors on request.

Conflicts of Interest: The authors declare no conflicts of interest.

References

1. Sharif, S.M.A.; Naqvi, R.A.; Biswas, M.; Loh, W.-K. Deep perceptual enhancement for medical image analysis. *IEEE J. Biomed. Health Inform.* **2022**, *26*, 4826–4836. [CrossRef] [PubMed]
2. Jie, Y.; Li, X.; Zhou, F.; Ye, T. Tri-Modal Medical Image Fusion and Denoising Based on BitonicX Filtering. *IEEE Trans. Instrum. Meas.* **2023**, *72*, 1–15. [CrossRef]
3. Pethuraj, M.S.; Burhanuddin, M.A.; Devi, V.B. Improving accuracy of medical data handling and processing using DCAF for IoT-based healthcare scenarios. *Biomed. Signal Process. Control.* **2023**, *86*, 105294. [CrossRef]
4. Khader, F.; Müller-Franzes, G.; Arasteh, S.T.; Han, T.; Haarburger, C.; Schulze-Hagen, M.; Schad, P.; Engelhardt, S.; Baeßler, B.; Foersch, S.; et al. Denoising diffusion probabilistic models for 3D medical image generation. *Sci. Rep.* **2023**, *13*, 7303. [CrossRef]
5. Son, Y.; Jeong, S.; Hong, Y.; Lee, J.; Jeon, B.; Choi, H.; Kim, J.; Shim, H. Improvement in Image Quality of Low-Dose CT of Canines with Generative Adversarial Network of Anti-Aliasing Generator and Multi-Scale Discriminator. *Bioengineering* **2024**, *11*, 944. [CrossRef]

6. Laghrib, A.; Afraites, L. Image denoising based on a variable spatially exponent PDE. *Appl. Comput. Harmon. Anal.* **2024**, *68*, 101608. [CrossRef]
7. Hu, R.; Xie, Y.; Zhang, L.; Liu, L.; Luo, H.; Wu, R.; Luo, D.; Liu, Z.; Hu, Z. A two-stage deep-learning framework for CT denoising based on a clinically structure-unaligned paired data set. *Quant. Imaging Med. Surg.* **2024**, *14*, 335–351. [CrossRef]
8. Oh, J.; Wu, D.; Hong, B.; Lee, D.; Kang, M.; Li, Q.; Kim, K. Texture-preserving low dose CT image denoising using Pearson divergence. *Phys. Med. Biol.* **2024**, *69*, 115021. [CrossRef]
9. Marcos, L.; Babyn, P.; Alirezaie, J. Generative AI in Medical Imaging and Its Application in Low Dose Computed Tomography (CT) Image Denoising. In *Applications of Generative AI*; Springer International Publishing: Cham, Switzerland, 2024; pp. 387–401.
10. Hou, R.; Li, F. IDPCNN: Iterative denoising and projecting CNN for MRI reconstruction. *J. Comput. Appl. Math.* **2021**, *406*, 113973. [CrossRef]
11. Xu, Z.; Wang, J.; Hu, F.; Abbas, G.; Touti, E.; Albekairi, M.; El-Hamrawy, O.I. Improved camouflaged detection in the large-scale images and videos with minimum boundary contrast in detection technique. *Expert Syst. Appl.* **2024**, *249*, 123558. [CrossRef]
12. Kakigi, T.; Sakamoto, R.; Tagawa, H.; Kuriyama, S.; Goto, Y.; Nambu, M.; Sagawa, H.; Numamoto, H.; Miyake, K.K.; Saga, T.; et al. Diagnostic advantage of thin slice 2D MRI and multiplanar reconstruction of the knee joint using deep learning based denoising approach. *Sci. Rep.* **2022**, *12*, 10362. [CrossRef] [PubMed]
13. Lei, Y.; Niu, C.; Zhang, J.; Wang, G.; Shan, H. CT Image Denoising and Deblurring With Deep Learning: Current Status and Perspectives. *IEEE Trans. Radiat. Plasma Med. Sci.* **2023**, *8*, 153–172. [CrossRef]
14. Fu, Y.; Dong, S.; Huang, Y.; Niu, M.; Ni, C.; Yu, L.; Shi, K.; Yao, Z.; Zhuo, C. MPGAN: Multi Pareto Generative Adversarial Network for the denoising and quantitative analysis of low-dose PET images of human brain. *Med. Image Anal.* **2024**, *98*, 103306. [CrossRef] [PubMed]
15. Hadri, A.; Laghrib, A.; El Mourabit, I. A new learning space-variant anisotropic constrained-PDE for image denoising. *Appl. Math. Model.* **2024**, *125*, 139–163. [CrossRef]
16. Wang, J.; Hu, F.; Abbas, G.; Albekairi, M.; Rashid, N. Enhancing image categorization with the quantized object recognition model in surveillance systems. *Expert Syst. Appl.* **2024**, *238*, 122240. [CrossRef]
17. Izadi, S.; Sutton, D.; Hamarneh, G. Image denoising in the deep learning era. *Artif. Intell. Rev.* **2023**, *56*, 5929–5974. [CrossRef]
18. Oshima, S.; Fushimi, Y.; Miyake, K.K.; Nakajima, S.; Sakata, A.; Okuchi, S.; Hinoda, T.; Otani, S.; Numamoto, H.; Fujimoto, K.; et al. Denoising approach with deep learning-based reconstruction for neuromelanin-sensitive MRI: Image quality and diagnostic performance. *Jpn. J. Radiol.* **2023**, *41*, 1216–1225. [CrossRef]
19. Wang, J.; Alshahir, A.; Abbas, G.; Kaaniche, K.; Albekairi, M.; Alshahr, S.; Aljarallah, W.; Sahbani, A.; Nowakowski, G.; Sieja, M. A deep recurrent learning-based region-focused feature detection for enhanced target detection in multi-object media. *Sensors* **2023**, *23*, 7556. [CrossRef]
20. Huang, Z.; Zhang, J.; Zhang, Y.; Shan, H. DU-GAN: Generative adversarial networks with dual-domain U-Net-based discriminators for low-dose CT denoising. *IEEE Trans. Instrum. Meas.* **2021**, *71*, 1–12. [CrossRef]
21. Wang, G.; Li, W.; Du, J.; Xiao, B.; Gao, X. Medical image fusion and denoising algorithm based on a decomposition model of hybrid variation-sparse representation. *IEEE J. Biomed. Health Inform.* **2022**, *26*, 5584–5595. [CrossRef]
22. Geng, M.; Meng, X.; Zhu, L.; Jiang, Z.; Gao, M.; Huang, Z.; Qiu, B.; Hu, Y.; Zhang, Y.; Ren, Q.; et al. Triplet cross-fusion learning for unpaired image denoising in optical coherence tomography. *IEEE Trans. Med. Imaging* **2022**, *41*, 3357–3372. [CrossRef] [PubMed]
23. Li, J.; Guan, W. Patch merging refiner embedding UNet for image denoising. *Inf. Sci.* **2023**, *641*. [CrossRef]
24. Liu, J.; Jiang, H.; Ning, F.; Li, M.; Pang, W. DFSNE-Net: Deviant feature sensitive noise estimate network for low-dose CT denoising. *Comput. Biol. Med.* **2022**, *149*, 106061. [CrossRef]
25. Alabdulhafith, M.; Othmen, S.; Alfahid, A.; Lhioui, C.; Abbas, G.; Hamdaoui, R.; Mobarak, W.; Aboelmagd, Y. Implementing a Transfer Learning for User Behavior Analysis and Prediction using Preference-dependent Model. *IEEE Access* **2024**, *12*, 82647–82659. [CrossRef]
26. Lu, Z.; Jia, S.; Li, G.; Jing, S. Neutron image denoising method based on adaptive new wavelet threshold function. *Nucl. Instrum. Methods Phys. Res. Sect. A Accel. Spectrometers, Detect. Assoc. Equip.* **2024**, *1059*, 169006. [CrossRef]
27. Xiao, G.; Wang, H.; Shen, J.; Chen, Z.; Zhang, Z. An Adaptive Hierarchical Concatenated Network With A Robust Loss Function For Image Denoising. *J. Grid Comput.* **2022**, *20*, 9. [CrossRef]
28. Okuwobi, I.P.; Ding, Z.; Wan, J.; Jiang, J. SWM-DE: Statistical wavelet model for joint denoising and enhancement for multimodal medical images. *Med. Nov. Technol. Devices* **2023**, *18*, 100234. [CrossRef]
29. Wang, S.; Lv, J.; He, Z.; Liang, D.; Chen, Y.; Zhang, M.; Liu, Q. Denoising auto-encoding priors in undecimated wavelet domain for MR image reconstruction. *Neurocomputing* **2021**, *437*, 325–338. [CrossRef]
30. Guo, G. Real-time medical image denoising and information hiding model based on deep wavelet multiscale autonomous unmanned analysis. *Soft Comput.* **2023**, *27*, 4263–4278. [CrossRef]
31. Wang, Y.; Han, Z.; Zhang, X.; Shangguan, H.; Zhang, P.; Li, J.; Xiao, N. Scale-sensitive Generative Adversarial Network for Low-Dose CT Image Denoising. *IEEE Access* **2024**, *12*, 98693–98706. [CrossRef]
32. Chao, L.; Wang, Y.; Zhang, T.; Shan, W.; Zhang, H.; Wang, Z.; Li, Q. Joint denoising and interpolating network for low-dose cone-beam CT reconstruction under hybrid dose-reduction strategy. *Comput. Biol. Med.* **2024**, *168*, 107830. [CrossRef] [PubMed]
33. El-Shafai, W.; El-Nabi, S.A.; Ali, A.M.; El-Rabaie, E.-S.M.; El-Samie, F.E.A. Traditional and deep-learning-based denoising methods for medical images. *Multimedia Tools Appl.* **2024**, *83*, 52061–52088. [CrossRef]

34. Kyung, S.; Won, J.; Pak, S.; Kim, S.; Lee, S.; Park, K.; Hong, G.S.; Kim, N. Generative Adversarial Network with Robust Dis-criminator Through Multi-Task Learning for Low-Dose CT Denoising. *IEEE Trans. Med. Imaging* **2024**. [CrossRef]
35. Song, Y.; Liu, Y.; Lin, Z.; Zhou, J.; Li, D.; Zhou, T.; Leung, M.-F. Learning From AI-Generated Annotations for Medical Image Segmentation. *IEEE Trans. Consum. Electron.* **2024**. [CrossRef]
36. Farooq, Y.; Savaş, S. Noise removal from the image using convolutional neural networks-based denoising auto en-coder. *J. Emerg. Comput. Technol.* **2024**, *3*, 21–28. [CrossRef]
37. Mohanapriya, G.; Muthukumar, S.; Shanmugapriya, M.M. Kalman Bucy Filtered Neuro Fuzzy Image Denoising for Medical Image Processing. *Neutrosophic Sets Syst.* **2024**, *70*, 314–330.
38. Radke, K.L.; Kamp, B.; Adriaenssens, V.; Stabinska, J.; Gallinnis, P.; Wittsack, H.J.; Antoch, G.; Müller-Lutz, A. Deep Learning-Based Denoising of CEST MR Data: A Feasibility Study on Applying Synthetic Phantoms in Medical Imaging. *Diagnostics* **2023**, *13*, 3326. [CrossRef]